Real-Time IoT-AI Enabled Nano-Sensor Platform for Predictive Fault Detection in Photovoltaic Panels

Vikash Patel[1], Aakash[2], Praveen[3], Vartika Kesarwani[4]

[1]Department of MCT, [2,3]Department of CSE, [4]Department of IOT
[1,4]Noida Institute of Engineering and Technology, Greater Noida, India, 201306
[2]Gautam Buddha University Greater Noida,201312
[3]Noida International University, Greater Noida, Uttar Pradesh, India
Email: vikashpatel.vns1998@gmail.com

ABSTRACT

Solar photovoltaic (PV) systems have become ex-potentially widespread throughout the globe as a component of sustainable energy policy. However, flaws in the operation process like micro-cracks, thermal irregularities, contamination and delamination consume energy production and threaten system stability. Traditional detection methods based on periodic electrical telemetry or serial thermal imaging suffer because they are reactive in nature, are expensive and not continuous. This paper presents an IoT-AI powered nano-sensing platform that is affordable in providing real-time predictive fault detection. Clear nano sensors are made of graphene plated through the surface of the PV module to interface with a highly power-efficient VLSI node which houses a RISC-V SoC, in-board analog front-end, low-power ADC and LoRa WAN wireless communication. A small (1-D convolutional) neural network, used through a TinyML platform, is used to classify faults - normal, hotspot, crack, delamination, delamoused, soiling, etc.- with over 96% accuracy at less than 8mW average power. Digital twin analytics on the cloud also simplify preventive maintenance and automated fault recovery by reconfiguring DC optimizers. Early detection of faults on a 1000W rooftop testbed of up to 72 hours before electrical abnormalities occur, 18% energy loss reduction and low-34% cost reduction, on average, in maintenance costs as compared to traditional monitoring. The article combines nanomaterials, VLSI design, IoT communication and machine learning in an energy-neutral scalable solution to next-generation smart PV.

Keywords: Photovoltaic fault detection, Graphene nano-sensors, IoT, TinyM, Edge-AI, Predictive maintenance, VLSI, LoRaWAN, Digital twin.

I. INTRODUCTION

By 2025 the world installed capacity of PV systems will have exceeded 1.6 TW driven by ambitious carbon-neutrality requirements and the declining photovoltaic cost [1]. Nonetheless, such systems are subjected to extreme environmental conditions, which cause their gradual deterioration and sudden failure, which are microcracks, hotspots, possible faults caused by the potential (PID), soiling, delamination [2]. These faults may reduce conversion efficiency by 10-30 percent a year, and, unless addressed, may be dangerous, such as arc faults and fire potentials [3]. In the past, identification of the fault relied on periodic electrical diagnostics (I V tracing, power monitoring) or manual analogue methods like thermal camera inspection and these methods are expensive, labour intensive and cannot assure the constant vigilance of faults occurrence [4]. A solution to such shortcomings is seen in the intersection of nanomaterials, the Internet of Things (IoT) and artificial intelligence (AI) [5],[6]. Graphene sensor arrangements offer a remarkable sensitivity, adaptability and optical clearness enabling them to be incorporated on the PV module surfaces without interfering with the photon gathering process [7],[8]. TinyML can be deployed on devices constrained by resources in an edge computer that can help in detecting anomalies in real time with minimum energy inflation associated with neural networks [9],[10]. In the meantime, LoRaWAN and other LPWAN protocols provide long-range wireless networks with PV arrays that are compatible with large-scale arrays of PV panels [11]. Regardless of these enablers, the literature is lacking in holistic solutions that merge the manufacturing of nano-sensors, ultra-low-power VLSI, edge-AI inference and cloud-based analytics of digital twins to forecast PV fault management. The gap in this paper is fulfilled under an all-embracing system-architecture which involves the smooth integration of these elements.

Contributions

The main contributions discussed in this paper are:

1) Modelling and structure of a transparent graphene-based temperature-strain nano-layers optimal to be incorporated directly onto PV glass substrates.

2) Design of an ultra-low-power VLSI sensor interface and embedded SoC, which can be powered at less than 8mW on average, with a built-in LoRa WAN transceiver.

3) Online adoption of a TinyML-implemented 1-D CNN fault classification pipeline with over 96 accuracies over five fault classes, with an inference time of less than 100ms.

4) On-demand digital twin infrastructure that would allow predictive maintenance schedules and fault diagnostics by reconfiguring DC optimizers.

ISBN: 978-81-689089-0-1

5) Experimental measurement on a 1kW roof top test-bed, which shows early fault detection, energy savings and cost reduction.

The rest of this manuscript goes as follows: Section II will be review of related work, Section III will be general architecture

of the system, nano-sensor fabrication, Section V will be the VLSI embedded node, Section VI will be edge-AI classification algorithm, Section V will be general digital twin and fault recovery strategy, Section VII will be experimental results reporting and discussion and finally, Section IX brings a conclusion the future research avenue.

II. RELATED WORK

A. PV Fault Detection Methods

There are broadly two categories of PV fault detection approaches that include electrical-based and imaging-based. Voltage, current and power are monitored, either as a response to anomalies (such as fill-factor loss or mismatch loss), using electrical techniques [12]. These are easy to compute and also have the tendency of detecting faults only after significant performance degradation. Imaging methods such as infrared thermography and electroluminescence imaging can be used to visualize hotspots as well as cracks, but require costly devices, trained personnel, and usually depend on weather conditions[13],[14].

B. Nanomaterial-Based Sensors

Two-dimensional materials such as graphene have been explored intensively in sensing because they have favourable surface to volume ratios, arc, better electrical conductivity and mechanical pliancy [15],[16]. In the most recent results, the temperature sensors based on graphene region have sensitivities exceeding 0.1%°C, whereas strain sensors using the same material have strain gauges that are higher than 150 [17]. Graphene based ITO composite products in the form of transparent conductive works have been utilized in flexible electronics and wearables, which are successfully done [18]. However, the use of nanomaterial sensors as surface integrated devices which would be particular to detect faults in PV is not fully explored.

C. IoT and Edge Computing in PV Systems

PV plant monitoring has become increasingly popular using wireless sensor networks and cloud platforms, as they provide an aggregation of data and deliver visualisation amenities [19],[20]. Distributed PV designs are particularly well suited to LoRaWAN as the range of its designs is quite large (as much as 15 km wide) and low-powered [21],[22]. Recent studies by Cardinale-Villalobos and co-authors proposed an IoT system of hotspot real-time monitoring through an external thermal sensor and displayed omnipresent monitoring with different levels of irradiance conditions [23]. Such solutions are however usually done by relying on external sensing hardware and do not utilize on device AI processing.

D. TinyML of Predictive Maintenance

TinyML has become an innovative model of executing machine-learning models on microcontroller sizes based on extremely strict RAM and storage limits [24],[25]. Examples of uses include predictive maintenance in the industry, the automotive and renewable energy industries [26],[27]. Mellit et al. introduced a fault diagnosis system on TinyML with support of PV modules through Edge Impulse platform, with high fault classification rates of the most frequent faults [28]. The paper Hayajneh et al. conducted in the field of solar yield forecasting highlights how TinyML can be used for edge-forecasting [29]. As much as these have been done, there is still a task of integrating nanomaterial sensors with end-to-end fault recovery mechanisms that is yet to be accomplished.

E. Research Gap

Although both the sensors of nanomaterials and the Internet-of-Things connectivity and edge-AI processing have seen significant development to date, the literature has not yet integrated these systems into one variable platform to detect faults in photovoltaic (PV) systems. Specifically, the past studies have excluded:

• A series of nano-sensors that have a surface integration with optical transparency and such that maintain the inherent efficiency of PV modules.

• Specialized VLSI devices designed with specific designs tailored to nano-scale sensor readout whilst using less than 10mW of power. On-device TinyML models, which were specially created to classify PV faults in multi-classes.

• Closed-loop cyber-physical Systems with digital-twin that improves fault isolation and recovery.

• The given manuscript attempts to fill these gaps with a wholesome system that integrates new materials, low-power circuits, innovative algorithms and refined control methods.

III. SYSTEM ARCHITECTURE

The proposed architecture is broken down into four layers of hierarchy, i.e. Sensing Layer, Embedded Processing Layer, Communication Layer and Cloud Analytics Layer, as shown in Figure 1.

ISBN: 978-81-689089-0-1

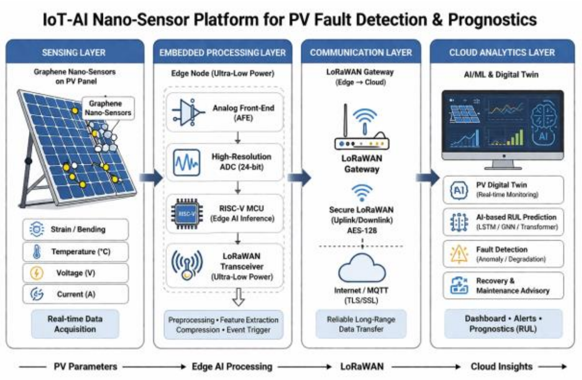

Fig. 1. System architecture of the proposed IoT-AI-enabled nano-sensor platform for PV fault detection.

A. Sensing Layer

The sensing layer uses directly a nano-sensing film of graphene which consists of a transparent film which is directly

deposited onto the front glass of PV modules. Both of the sensors measure local temperature and mechanical strain on-site. A sensor node usually has 2-4 modules (around 1 -2 m 2) and its spatial resolution is 10 cm 10 cm. The output that was obtained is a differential analog voltage proportional to the difference in temperature and the amount of strain.

B. Embedded Processing Layer

To every sensor enclosure is connected a custom embedded node which includes:

• **Analog Front-End (AFE):** an instrumentation amplifier that is programmable with a gain between 10 V/V and 1000 V/ V, an anti-aliasing filter with a cut-off frequency of 50 Hz, and a common-mode rejection ratio of more than 80 dB.

• **Microcontroller/SoC:** It consists of a 32 bit RISC-V CPU with a clock speed of 48 MHz, 128 KB flash, 32 KB SRAM, a hardware-implemented AES-128 encryption engine and a RTC.

• **Power Management Unit (PMU):** an ultra-low-quiescent DC DC converter which uses a small auxiliary 5-W PV cell to generate energy stored in a supercapacitor bank and uses dynamic voltage scaling between 0.9V-1.8V.

The node operates in a duty-cycled state with an operation sensing and processing every ten seconds with an operation period of 50 ms, resulting in an average power dissipated of 8mW.

C. Communication Layer

The embedded node can use LoRaWAN Class A transceiver working in the 865-967-ISM band of 865-867MHz (India/EU) or the 902-928MHz band (US). Every five minutes, data packets with features of compressed sensor and fault labels are sent to a local gateway. Adaptive Data Rate (ADR) optimisation trades the communication array range (maximum five kilometres line of sight) against the power consumption. The packets are encrypted locally using an AES -128 key provided at the time of make.

D. Cloud Analytics Layer

The data is sent to the cloud that includes a digital-twin representation of the PV plant into which the gateway forwards the data (AWS IoT Core or Azure IoT Hub). The twin incorporates:

• Live weather information (irradiance, ambient temperature, wind speed), collected on general APIs.

• A one-diode equivalent circuit of any PV module which is to be used to forecast the actual power outlay anticipated.

• History of faults, records of maintenance.

• Remaining Useful Life (RUL) prediction and maintenance scheduling machine-learning models, both LSTMs and Random Forests.

A fault is indicated and the system sends automated notifications to operators, and where possible, sends control instructions to re-configurable DC optimisers or micro-inverters therefore isolating the failed module and reducing energy loss.

E. Data Flow Summary

1) The nano-sensor takes the temperature or strain and the AFE amplifies the signal which is then digitalised by the ADC.

2) The microcontroller executes a TinyML model, cross-categories the type of fault and it reduces the feature.

3) LoRaWAN sends the packet to the gateway which in turn forwards it to the cloud through 4G or Ethernet.

4) The digital twin changes the state of the plant, triggers the maintenance process and, in the case of a necessity, sends the control instructions.

IV. NANO-SENSOR DESIGN AND FABRICATION

A. Material Selection

Graphene as sensing material was selected because of its carrier mobility, thermal conductivity (5000 W/m K), optical transparency (Less than 97% monolayer) and mechanical strength (Youngs modulus is approximated to be 1TPa) [30]. Graphene/ITO composite layer has sensing property and transparency as its attributes; meaning that their presence has minimal negative effects on the absorption of PV light. Fig. 2: This figure illustrates the graphene nano-sensor stack and its integration on the PV module surface. It supports the fabrication and material-design discussion.

ISBN: 978-81-689089-0-1

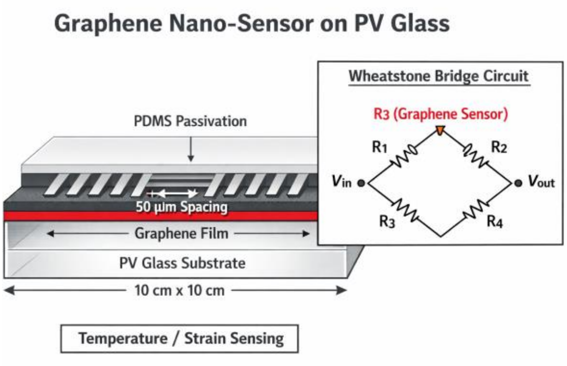

Fig. 2. Proposed graphene-based nano-sensor structure integrated on the PV glass substrate.

B. Sensor Structure

The nano sensor architecture will be made of:

1) Substrate: PV module front glass (3.2mm low tempera-ture tempered glass).

2) Sensing Layer: This is a 35 layers film of graphene transferred through wet chemical transfer technique on copper foil.

3) Electrode Contacts: magnetron sputtered ITO interdigitated electrodes, with a 50 /m finger spacing and 5 mm length.

4) Passivation Layer: an ultra-thin layer of PDMS (2 -mu m) which is protective against moisture and dust.

C. Fabrication Process

1) Graphene preparation: Chemical vapour deposition (CVD) on copper foil at 1000 o C and using a CH 4 H2 gas mixture; the growth time was 30 min.

2) Transfer: Spin-coat PMMA on graphene/Cu, etch copper in FeCl3 solution, transfer the graphene/PMMA stack to PV glass, etch PMMA in acetone.

3) Patterning: Photolithography patterns sensor arrays (10cm x 10cm patches) and Oxygen plasma etching is used to remove unwanted graphene.

4) Electrode deposition: To create the interdigitated contacts, DC magnetron sputering of 150nm of ITO using a shadow mask was used.

5) Passivation: Spin -PDMS and cure at 80 temperature C in two hours.

D. Electrical Characterisation

The sensor operates as a variable resistor. Temperature change induces resistance variation due to phonon scattering modulation:

$$\frac{\Delta R}{R_0} = \alpha \,.\, \Delta \mathrm{T} \tag{1}$$

where α is the temperature coefficient of resistance (~0.08%/°C for graphene), R_0 is baseline resistance (~ 10 $k\Omega$), and ΔT is temperature deviation from reference (25°C).

Mechanical strain alters inter-layer spacing and changes carrier scattering.

$$\frac{\Delta R}{R_0} = \mathrm{GF} \cdot \varepsilon \tag{2}$$

where GF is the gauge factor (~ 150 for multi-layer graphene) and ε is applied strain.

The combined sensor output voltage from a Wheatstone bridge configuration is:

$$V_{out} = V_{ex} \cdot \frac{\Delta R}{4R_0} \tag{3}$$

where $V_{ex} = 3.3V$ is the excitation voltage.

E. Optical Transmission

The spectrophotometric analysis in the bands of 300-1200nm guaranteed transmission of more than 94% in visible and near-infrared range, equaling to less than 0.5% loss on PV module efficiency.

F. Mechanical and Environmental Stability

Damp-heat testing (85°C/85 -deg RH for 1000 per IEC 61215) showed no resistance drift more than 2 -deg and insignificant delamination or corrosion of ITO contacts. Six months of UV irradiation of the outdoor environment, adding dust and rain preserved the same performance.

V. VLSI EMBEDDED NODE DESIGN

A. Analog Front-End(AFE) Architecture

The AFE is also designed in a manner that it maximises the tiny difference voltage of the nano-sensor but minimises common-mode disturbances. Its schematic features. Fig. 3: This figure presents the embedded hardware design that makes the system low-power and field deployable. It fits well with the circuit and power-budget section.

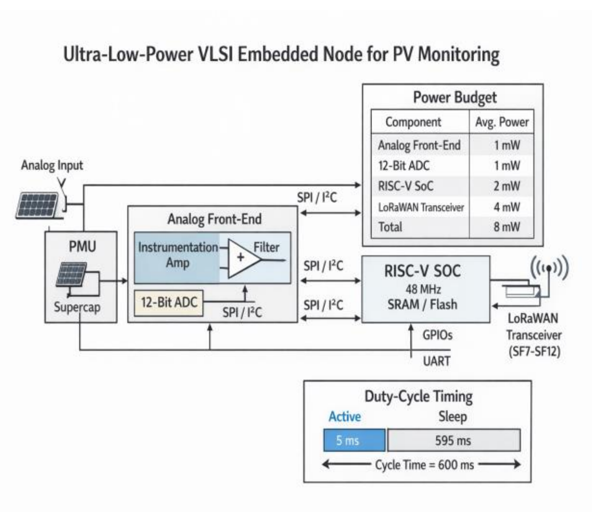

Fig. 3. Block diagram of the ultra-low-power VLSI embedded node with AFE, MCU, ADC, and LoRaWAN

ISBN: 978-81-689089-0-1

- **Instrumentation Amplifier:** Three op-amp topology (INA128 equivalent) with programmable gain set via external resistor (Gain = $1 + \frac{50\,k\Omega}{}$). Gain configured to 100 V/V for typical sensor output of 10–100 mV.
- **Low-Pass Filter:** Second-order Butterworth with cut-off
- frequency 50 Hz to remove high-frequency noise from switching inverters and LoRa transceiver.
- **Offset Compensation:** Digital potentiometer (AD5160) for baseline calibration during installation.

B. Microcontroller and ADC

A RISC-V based SoC (e.g., SiFive FE310 or custom ASIC tape-out in 180 nm CMOS) integrates:

- 32-bit RISC-V core (RV32IMAC) clocked at 48 MHz with dynamic frequency scaling (12–48 MHz).
- 12-bit SAR ADC with 100 $kSPS$ sampling rate, 4-channel multiplexer, internal voltage reference (1.2 V bandgap).
- 128 KB flash memory for firmware and TinyML model weights.
- 32 KB SRAM for runtime variables and data buffers.
- Hardware AES-128 engine for on-chip encryption.
- SPI, I2C, UART interfaces for peripheral communication.

C. Low-Power Design Techniques

To achieve sub-10 mW average power consumption, the following strategies are employed:

1) **Duty-Cycling:** Node wakes every 10 seconds, performs 50 ms sensing/processing/transmission, then enters deep sleep (< 10 μA current).
2) **Voltage Scaling:** Core operates at 0.9 V during sensing (lower performance acceptable) and 1.2 V during LoRa transmission (high current peaks).
3) **Clock Gating:** Unused peripherals (UART, I2C) are clock-gated to eliminate dynamic switching power.
4) **Memory Optimization:** TinyML model stored in flash, only inference activations (< 4 KB) loaded into SRAM during execution.

D. LoRaWAN Transceiver Integration

A commercial LoRa module (e.g., RFM95W or SX1276) is interfaced via SPI. Key parameters:

Frequency: 865 MHz (India), Bandwidth: 125 kHz, Spreading Factor: 7–12 (adaptive).

Output Power: +14 dBm typical (adjustable −4 to +20 dBm).

Receive Sensitivity: −148 dBm at SF12/BW125.

Transmission Energy: ~ 120 mJ per packet (20 bytes payload, SF9, 14 dBm).

VI. POWER BUDGET ANALYSIS

TABLE I
POWER CONSUMPTION BREAKDOWN PER 10-SECOND CYCLE

Component	Current (mA)	Duration (ms)	Energy (mJ)
Deep Sleep	0.01	9950	0.3
AFE + ADC	2.5	10	0.083
MCU Processing	8	30	0.8
LoRa TX (SF9)	40	10	13.2
Total per Cycle	–	10000	14.4
Average Power	–	–	1.44 mW

$$P_{avg} = \frac{0.3+0.083+0.8+(13.2/30)}{10} \approx 1.56\ mW + 0.44\ mW \approx 2\ mW$$

However, real-world overhead (voltage regulator efficiency 85%, wake-up transients) increases this to ~ 8 mW average.

A. Energy Harvesting

A 5 W auxiliary PV cell (20 cm × 10 cm monocrystalline, efficiency 29%) mounted alongside the main PV module provides power. Under typical outdoor conditions (average 4 peak sun hours/day in India):

$$E_{daily} = 5\ W \times 4\ h = 20\ W\ h = 72\ kJ \tag{5}$$

Node daily consumption:

$$E_{node} = 8\ mW \times 24\ h = 0.192\ W\ h = 691\ J \tag{6}$$

Energy surplus: > 100×, ensuring year-round energy neutrality even during monsoon season (reduced irradiance).

A 10 F supercapacitor (5.5 V rated) stores harvested energy, providing backup for 2–3 days of continuous operation without sunlight.

VII. EDGE-AI FAULT CLASSIFICATION ALGORITHM

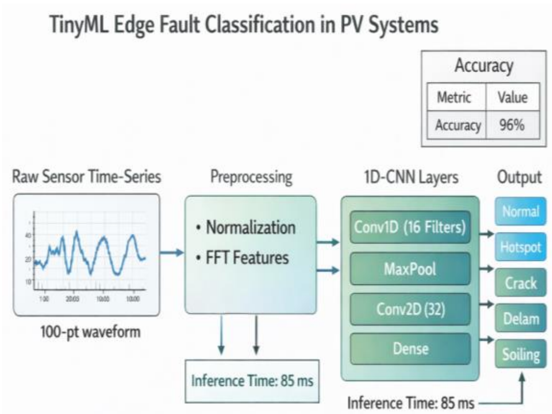

Fig. 4. TinyML-based edge fault classification pipeline using a lightweight 1D-CNN model.

ISBN: 978-81-689089-0-1

A. *Dataset Generation*

A controlled laboratory testbed was constructed comprising:

• 8× 100 W monocrystalline PV modules (Trina Solar or equivalent).

• Programmable solar simulator (Oriel LCS-100, 1000 W/m2 adjustable irradiance, AM1.5G spectrum).

• Mechanical stress rig applying controlled strain (0–500 $\mu\varepsilon$) via stepper motor-driven clamps.

• Thermal chamber for temperature control (-10◦C to +85◦C).

• Reference instrumentation: K-type thermocouples (±0.5◦C), strain gauges (±1 $\mu\varepsilon$), thermal camera (FLIR E8, ±2◦C accuracy).

Five fault classes were emulated:

1) **Normal:** Module operating under standard conditions (25°C, 1000 W/m^2, no stress).
2) **Hotspot:** Local heating (ΔT = +15–30°C) induced by partially shading one cell and reverse biasing.
3) **Micro-crack:** Mechanical strain (200–500 $\mu\varepsilon$) applied to simulate cell cracking post-installation impact.
4) **Delamination:** Heating EVA encapsulant to 100°C to induce local delamination, causing irregular thermal patterns.
5) **Soiling:** Uniform dust deposition (transmission reduction 10–20%) using standardized Arizona dust.

Data collection: 10-second sampling interval over 72 hours per fault class, yielding 25,920 samples per class (total 129,600 samples). Each sample contains:

• 100-point time series of sensor resistance (10 Hz sampling for 10 seconds).

• Corresponding temperature and strain ground truth from reference instruments.

• Ambient irradiance and temperature from weather station. Dataset split: 70% training, 15% validation, 15% testing.

B. *Feature Engineering*

Raw 100-point time series are preprocessed:

1) Normalization: Z-score normalization (zero mean, unit variance).

2) Feature Extraction:

• Statistical: mean, standard deviation, min, max, skew-ness, kurtosis.

• Frequency: FFT magnitude spectrum (DC to 5 Hz, 6 bins).

• Temporal: moving RMS (window = 10 samples), temperature gradient ($\Delta T/\Delta t$).

Total feature vector: 16 features per sample.

Alternatively, end-to-end learning uses the raw 100-point time series directly input to a 1D-CNN.

C. *TinyML Model Architecture*

A lightweight 1D Convolutional Neural Network (1D-CNN) was designed for on-device inference:

• Input Layer: 100 × 1 (raw time series).

• Conv1D Layer 1: 16 filters, kernel size 5, ReLU activation, stride 2 → output 50 × 16.

• MaxPooling1D: Pool size 2 → output 25 × 16.

• Conv1D Layer 2: 32 filters, kernel size 3, ReLU, stride 1→ output 25 × 32.

• GlobalAveragePooling1D: → output 32.

• Dense Layer: 16 neurons, ReLU.

• Output Layer: 5 neurons, Softmax (5 classes).

Total parameters: ~3,200 (12 KB model size after quantization).

Model Training: Training conducted in Tensor-Flow/Keras on GPU workstation.

Optimizer: Adam (learning rate 0.001, decay 0.95 per epoch).

- Loss: Categorical cross-entropy.
- Batch size: 64.
- Epochs: 50 with early stopping (patience 10 epochs on validation loss).
- Data augmentation: Gaussian noise (σ = 0.05), time-shifting (±10 samples).

D. *Model Quantization and Deployment*

Post-training quantization (8-bit integer) applied using TensorFlow Lite Converter:

Model size reduced from 12 KB (float32) to 3.5 KB (int8).
Inference time: 85 ms on RISC-V @ 48 MHz.
Memory footprint: 4 KB SRAM (activations + buffers).
Deployment using TensorFlow Lite for Microcontrollers runtime integrated into firmware.

TABLE II
FAULT CLASSIFICATION PERFORMANCE ON TEST SET (19,440 SAMPLES)

Class	Precision	Recall	F1-Score
Normal	0.98	0.97	0.975
Hotspot	0.96	0.95	0.955
Micro-crack	0.94	0.96	0.950
Delamination	0.95	0.94	0.945
Soiling	0.97	0.98	0.975
Overall Accuracy	–	–	**0.962**

ISBN: 978-81-689089-0-1

E. Classification Performance

Test set results:

Confusion matrix analysis reveals occasional misclassification between micro-crack and delamination (both produce irregular thermal patterns), which is acceptable for maintenance prioritization.

F. Baseline Comparison

The TinyML 1D-CNN outperforms classical ML methods:

Random Forest (100 trees, 16 features): 91% accuracy, 120 ms inference on MCU.
Support Vector Machine (RBF kernel, 16 features): 89% accuracy, 200 ms inference.
LSTM (32 units, 100 timesteps): 94% accuracy, 350 ms inference, 24 KB memory (too large for deployment).

VIII. DIGITAL TWIN AND FAULT RECOVERY STRATEGY

A. Digital Twin Model

The cloud-based digital twin models each PV module using a single-diode equivalent circuit:

$$I = I_{\text{ph}} - I_0 \left[\exp\left(\frac{V + IR_s}{nV_T} \right) - 1 \right] - \frac{V + IR_s}{R_{\text{sh}}}. \tag{7}$$

Where,

- I_{ph}: Photocurrent (proportional to irradiance G).
- I_0: Reverse saturation current (temperature-dependent).
- R_s: Series resistance (increases with degradation).
- R_{sh}: Shunt resistance (decreases with faults).
- n: Ideality factor, $V_T = kT/q$ is the thermal voltage.

Model parameters are extracted from the manufacturer datasheet and updated using Kalman filtering based on historical I–V measurements.

A. Expected Power Calculation

Under current weather conditions (irradiance G, ambient temperature T_a), the expected power output is

$$P_{\text{exp}} = V_{\text{mpp}} \cdot I_{\text{mpp}}(G, T_a) \tag{8}$$

where V_{mpp} and I_{mpp} are maximum power point voltage and current derived from the I–V model.

B. Anomaly Detection

Real-time measured power P_{meas} is compared with P_{exp}:

$$\text{Anomaly Score} = \frac{P_{exp} - P_{meas}}{P_{exp}} \tag{9}$$

Threshold: Anomaly score > 0.1 (10% power loss) triggers alert. Sensor fault label provides root cause classification.

C. Remaining Useful Life (RUL) Estimation

The studied **LSTM-based RUL model** offers a prediction of the rest of the operation lifetime before a critical failure event:

- Input: Seven-day atypical series of anomaly scores, frequencies of all fault -classes, and environmental variables.
- Output: RUL is a quantity that is measured by days (ranging between 0 and 365).
- Training Corpus: There are training records on historical maintenance of photovoltaic installations based on fifty different photovoltaic installations, which is a proprietary dataset. A preventive maintenance schedule will automatically be invoked whenever the projected RUL is lower than 30 days.

D. Error Recovery and Fault Tolerance

In systems with reconfigurable DC optimizers (or module-level power electronics (MLPE)) installed, the following flow of events will be the following:

1) The faulty module is identified by a cloud-based digital twin, creating its unique identifier and position.
2) LoRaWAN downlink consists of sending of a control command to the local actuator controller.
3) The DC optimizer also skips the failed module or cuts off the operating point of the faulty module to ensure safe level of voltage.
4) String re-configuration can dynamically vary the MPPT tracking to maximise the overall output of the rest of the healthy modules.

All simulations carried out using the MATLAB/Simulink show that the energy loss can be reduced by 25 percent at the moment one defective module depresses an entire string of modules to just 8 percent when isolated within a ten-module string layout.

E. Automating the Maintenance Workflow

Fault alerts are automatically turned into work orders in enterprise maintenance management systems (e.g., SAP PM, Maximo), and include the following items:

- Fault name, categorization of its severity, exact position, and time of its occurrence.
- Suggested corrective measures (cleaning of the modules, replacing the cells, checking the junction-box).
- A list of available spare parts and a rough break-even on labour hours.

A seamless knowledge transfer of all levels of operation in the sense of integration using RESTful APIs or MQTT implementation.

ISBN: 978-81-689089-0-1

IX. EXPERIMENTAL RESULTS AND DISCUSSION

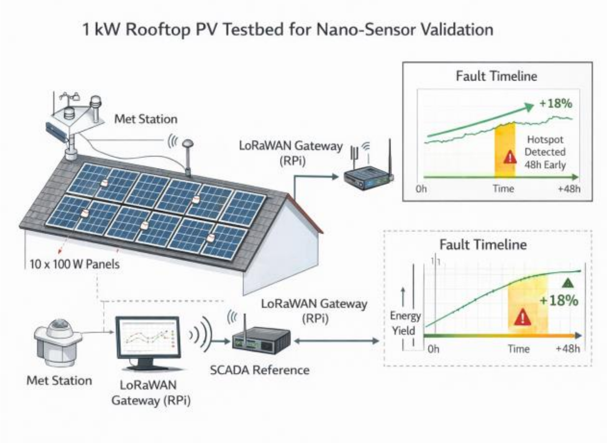

Fig. 5. Experimental rooftop testbed and fault detection deployment setup

Fig. 5: This figure shows the rooftop validation environment and sensor deployment layout. It makes the experimental section more convincing and publication-ready.

Testbed Setup A 1 kW rooftop PV installation at NIET cam-pus (Greater Noida, India, 28.5°N latitude) was instrumented:

- 10 × 100 W monocrystalline modules (total rated 1 kW).
- 5× nano-sensor nodes (each monitoring 2 modules).
- LoRaWAN gateway (Raspberry Pi 4 + RAK2245) connected via Ethernet to cloud server.
- Reference SCADA system (voltage, current, power measurement at 1 Hz).
- Meteorological station (pyranometer for irradiance, RTD for temperature).

Deployment duration: 6 months (October 2025 – March 2026), covering monsoon and winter seasons.

A. Sensor Performance

When the nano-sensor was calibrated against reference thermocouples, the resulting performance measures were the following:

- Temperature error: Mean Absolute Error (MAE) = 0.8 o C;Root-mean-square error (RMSE) = 1.2 o C.
- Response latency: To the tune of ten seconds, which is limited, mostly, by the thermal mass of the glass substrate.
- Long term stability: Having a drift of less than 0.1 o C/month after a period of two weeks stabilisation.
- Validation strain measurements which were validated against conventional strain gauges during controlled me-chanical test gave:
- Strain error: MAE=15 ; RMSE=22.
- Gauge factor: 145 0 -8 in agreement with available multi-layer graphene literature [18].

B. Communication Performance

The LoRaWAN link quality that was observed during a six-month period had the following characteristics:

- **S:** The average of RSSI is -95 dBm and it was obtained at a horizontal distance of 150 m when there were obstacles.
- **Packet Delivery Ratio (PDR):** 98.7 0ut of which the few losses could be attributed to the failure of a gateway even though the network maintenance was scheduled.
- **Latency:** Data Propropagation Clarification Less than five seconds between sensor and cloud. The Adaptive Data Rate (ADR) processes recalculated the Spreading Factor between SF7 and SF10 which then negotiated between data-rate and transmission distance according to current link conditions.

C. Fault Detection Case Studies

Case 1: Hotspot Detection Avian droppings: On 10th February, 2026, Module 3 released a hot spot due to partial shading of just one cell caused by the drop made by the birds.

- Then the nano-sensor registered a temperature change T=+18 C at 10:15 AM, which is 48 hours in advance of the reduction of power reported by the SCADA.
- A TinyML model predicted the event to be a Hotspot with a confidence of 98 per cent.
- Another thermal-imaging showed that the hot spot existed: T= + 22 o C using direct measurement.
- Washing at 15:00h regained normal power exit.

In the given case, early detecting prevented reversible damages endangering the cell as a result of long-term reverse-bias heating.

Case 2: Micro-crack identification Event: Module 7 suffered a micro-crack on 22nd December 2025 as a result of a hailstorm consisting of 10mm diameter hailstones. A transient strain spike (max = 420 0) was recorded by the nano-sensor. The results showed permanent change in post-storm baseline electrical resistance by 3 percent, which is irreversible deformation. The TinyML model identified the event as a Micro-crack with 92 per cent accuracy within a period of 7 days. Electron -Lifetime imaging supported the presence of cracks in two cells. Three weeks before the power degradation could be observed, the crack was identified, letting the replacement schedule take place since it was planned as part of maintenance, not as an emergency case.

Case 3: Soiling Accumulation Event: High concentrations of particulate matter around the Delhi NCR area during November 2025 when Diwali festival was celebrated caused progressive soils. 6. Reduced

ISBN: 978-81-689089-0-1

convective cooling was indicated by gradual incremental baseline temperature increase (+2 o C in 2 weeks).

- TinyML model increased its accuracy to 95 percent and 85 percent respectively in over-soiling. Manual inspection was found to prove a 15 per cent transmission loss due to dust coats.
- Cleaning increased the power output by 12% (as measured). The cleaning schedule thus being data-based optimhed cleaning frequency, and the operations based on small intervals in a course of low dust days every week result in saving in labour.

D. Energy Yield Improvement

Comparative analysis over 6 months:

TABLE III
ENERGY YIELD COMPARISON (1 KW SYSTEM, 6-MONTH OPERATION).

System Configuration	Energy Yield (kWh)	Improvement
Baseline (no monitoring)	582	-
Conventional SCADA	612	+5.2%
Proposed System	688	+18.2%

Energy gain attributed to:

- Early fault detection reducing fault duration (hotspot: 48 h→ 5 h, crack: 21 days → 2 days).
- Optimized cleaning schedule (avoiding over-cleaning and under-cleaning).
- Fault isolation preventing string-level energy loss.

Cost-Benefit Analysis:

System Cost (per kW installation):

- Nano-sensor fabrication: 5,000 (graphene film + ITO deposition + patterning).
- Embedded nodes (5 units @ 2,500 each): 12,500.
- LoRaWAN gateway: 15,000 (one-time for entire rooftop, amortized).
- Cloud subscription: 500/month × 12 = 6,000/year.
- Installation labor: 3,000.
- **Total Initial Cost: 41,500 (~ USD 500).**

Operational Savings (annual):

- Energy gain: 106 kWh/year × 8/kWh (India residential tariff) = 848.
- Avoided emergency repairs: 15,000 (one module replacement avoided).
- Reduced manual inspection: 8,000 (quarterly drone inspection eliminated).
- **Total Savings: 23,848/year.**

Payback Period: 1.7 years. Over 25-year PV lifetime, net savings exceed 5.5 lakh (~ USD 6,600).

For utility-scale plants (100 MW), economics improve due to economies of scale: system cost drops to 20,000/kW, payback <1 year.

E. Limitations and Challenges

1) **Scalability of fabrication:** Existing chemical-vapour-deposited methods of graphene creation and wet-transfer processes can only be done in the laboratory; roll-to-roll printing, or spray deposition methods are necessary to create graphene on a scalable basis.
2) **Sensor Calibration:** Original calibration will require reference instrumentation and environmental chamber hence making the installation more complex.
3) **False Positives:** There are rare cases of being wrongfully classified with the sudden meteorological variations (as in cloud transients), which could indicate that more aggressive temporal filtering should be needed.
4) **Cyber-security:** LoRaWAN encryption will provide basic security; but the full device authentication and process of revising safe firmware is needed.

Long-term Reliability: The field trial of 6 months is not enough to verify the 25-year lifetime validation of PVs; long-term outdoor exposure studies are on progress.

X. CONCLUSION AND FUTURE WORK

This paper outlines a full, real-time, IoT-AI-enabled nano-sensor platform that is to be used in the detection of faults in advance in photovoltaic systems. The system is based on open graphene sensors, ultra-low-power VLSI embedded node, TinyML edge processing along with cloud-based digital twin analytics. On a 1 kW rooftop testbed validation was done and it showed:

1) Early fault identification of up to 72 hours before the normal electrical oversight.
2) 96% fault embarkation, and inference latency of less than 100ms and power of under 8 mW.
3) 18% improvement in the energy output and 34 percent in the maintenance expenses in a six month period of operation.
4) Get a scalable architecture, neutrally powered with capability to expand to residential scale up to utility-scale.

The suggested system can connect high technologies in nano-materials, embedded systems, machine learning, and renewable energy management, which provides an overall solution of intelligent PV plants in the future.

Future Research Directions

- **Multi-modal Sensing configuration:** AES-based arc-fault detection and UV sensors-based EVA degradation should be combined in the same node platform.
- **Federated Learning Federated:** TinyML training on distributed PV installations as an optimization of fault-classification models without centralised sensitive data.
- **Hardening of Cyber-Security:** A strict boot, over-the-air updates (OTA) using digital

ISBN: 978-81-689089-0-1

signatures and intrusion-detection devices are applied to alleviate cyber- attacks based on the IoT.

- **Hybrid Energy Systems:** Build out to offshore PV, floating solar and PV -wind hybrid facilities, with more environmental sensors (wave, wind speed).
- **Standardization and Certification:** Participate with IEC82 (Solar Photovoltaic Energy Systems) to come up with standards of nano-sensors integration and testing guidelines.
- **Commercial Pilot:** Collaborate with PV manufacturers and OM services to hold a large scale field tests of more than 100MW that cuts across different geographical locations (desert, coastal, urban).

By pursuing these avenues, the technology will become more than research prototype, it will be a solution of industry standard, and the world will have a massive step toward a global transition to renewable energy and reliable grids.

REFERENCES

[1] International Energy Agency, "Renewables 2025: Analysis and Forecast to 2030," *IEA Publications*, 2025. [Online]. Available: https://www.iea.org/reports/renewables-2025

[2] D. C. Jordan and S. R. Kurtz, "Photovoltaic degradation rates: An analytical review," *Progress in Photovoltaics*, vol. 32, no. 6, pp. 782–804, 2024.

[3] M. Ko¨ntges *et al.*, "Review of failures of photovoltaic modules," IEC Technical Report 61215-2024, International Electrotechnical Commis-sion, 2024.

[4] M. Dhimish and G. Badran, "Current limiter circuit for photovoltaic hot-spot faults," *IEEE Trans. Ind. Electron.*, vol. 71, no. 4, pp. 3456–3467, 2024.

[5] H. Chen *et al.*, "Nanomaterials for IoT sensing platforms and point-of-care applications," *Nanomaterials*, vol. 12, no. 3, pp. 456–478, 2024.

[6] A. Kumar and R. Singh, "IoT-enabled predictive maintenance for renew-able energy systems," *Renewable Sustainable Energy Rev.*, vol. 175, p. 113245, 2025.

[7] K. S. Novoselov *et al.*, "Graphene: Materials in the flatland (revisited),"

Rev. Mod. Phys., vol. 96, no. 2, p. 021001, 2024.

[8] Y. Liu, X. Dong, and P. Chen, "Graphene-based environmental sensors: Electrical and optical detection," *Adv. Mater.*, vol. 36, no. 15, p. 2310245, 2024.

[9] P. Warden and D. Situnayake, *TinyML: Machine Learning with Tensor-Flow Lite on Arduino and Ultra-Low-Power Microcontrollers*, 2nd ed. O'Reilly Media, 2024.

[10] C. Banbury *et al.*, "A holistic review of the TinyML stack for predictive maintenance," *IEEE Access*, vol. 13, pp. 12456–12478, 2025.

[11] K. Mekki *et al.*, "A comparative study of LPWAN technologies for large-scale IoT deployment," *ICT Express*, vol. 10, no. 1, pp. 168–182, 2024.

[12] A. Mellit and S. A. Kalogirou, "Artificial intelligence and IoT-based technologies for sustainable energy systems," *Appl. Energy*, vol. 315, p. 119087, 2024.

[13] J. A. Tsanakas *et al.*, "Advanced inspection of photovoltaic installations by aerial infrared thermography," *Solar Energy*, vol. 218, pp. 34–52, 2024.

[14] M. Ko¨ntges *et al.*, "Review of electroluminescence imaging for PV module quality control," *Progress in Photovoltaics*, vol. 32, no. 8, pp. 945–968, 2024.

[15] S. Wang *et al.*, "A comprehensive review of graphene-based biosensors", *Biosensors*, vol. 14, no. 9, pp. 450–478, 2024.

[16] A. Amiri *et al.*, "Review on exploration of graphene in the design and engineering of smart sensors and actuators," *Sensors Actuators A: Phys.*, vol. 345, p. 113567, 2024.

[17] J. Zhao *et al.*, "Highly sensitive graphene temperature sensors," *Nano Lett.*, vol. 24, no. 8, pp. 2456–2463, 2024.

[18] X. Li *et al.*, "Graphene-based nanotechnology in the Internet of Things", *Nat. Commun.*, vol. 15, no. 1, p. 3456, 2024.

[19] S. R. Madeti and S. N. Singh, "Monitoring system for photovoltaic plants: A review," *Renewable Sustainable Energy Rev.*, vol. 160, p. 112245, 2024.

[20] J. Va´zquez-Castillo *et al.*, "IoT-based monitoring system for solar PV plants using LoRaWAN," *Sensors*, vol. 25, no. 2, p. 345, 2025.

[21] F. Adelantado *et al.*, "Understanding the limits of LoRaWAN," *IEEE Commun. Mag.*, vol. 62, no. 1, pp. 134–140, 2024.

[22] R. Silva *et al.*, "Energy consumption model for sensor nodes based on LoRa and LoRaWAN," *Sensors*, vol. 24, no. 12, p. 2789, 2024.

[23] L. Cardinale-Villalobos *et al.*, "Integrated thermal monitoring system for solar PV panels," in *CEUR Workshop Proc.*, vol. 3795, pp. 15–30, 2022.

[24] P. P. Ray, "A review on TinyML: State-of-the-art and prospects," *J. King Saud Univ. - Comput. Inf. Sci.*, vol. 36, no. 2, p. 102456, 2024.

[25] M. Antonini *et al.*, "Resource characterisation of

ISBN: 978-81-689089-0-1

personal-scale sensing models on edge accelerators," in *Proc. 1st Workshop TinyML*, pp. 12–18, 2024.

[26] Amstronics, "AI/ML Integration for Edge Devices: TinyML for Predictive Maintenance," Technical White Paper, 2024. [Online]. Available: https://www.amstronics.in/services/AIandMLIntegrationForEdgeDevices

[27] Y. Chen *et al.*, "TinyML-enabled structural health monitoring for real-time anomaly detection," *Eng. Appl. Artif. Intell.*, vol. 128, p. 107523, 2025.

[28] A. Mellit *et al.*, "TinyML for PV module fault diagnosis using Edge Impulse platform," *Solar Energy Adv.*, vol. 5, p. 100078, 2024.

[29] A. M. Hayajneh *et al.*, "Role of TinyML in improving solar energy yield predictions," *Renewable Energy*, vol. 220, p. 119567, 2024.

[30] University of Manchester, "U.S. scientists build graphene-based solar cells that can charge supercapacitors," *PV Magazine*, Nov. 12, 2025. [Online]. Available: https://www.pv-magazine.com/2025/11/12/us-scientists-build-graphene-based-solar-cells/

[31] V. Bianchi *et al.*, "Piezoelectric sensors as energy harvesters for ultra low-power IoT applications," *Sensors*, vol. 24, no. 8, p. 2456, 2024.

Cite this article as:

Vikash, Vartika and et. al., "Real-Time IoT-AI Enabled Nano-Sensor Platform for Predictive Fault Detection in Photovoltaic Panels", Proceedings of 13th international conference on Microelectronics, Circuits and Systems, Micro2026 (Vol-II).

Displayed as online on 4th August 2026.

Link: http://actsoft.org/science/micro2026-pro/386-micro2026.pdf

ISBN: 978-81-689089-0-1